# ANALYZING THE PERFORMANCE OF CIRCLE SEGMENT END MILL WITH PCD INSERTS WITH LASER-MACHINED INTEGRAL CHIPBREAKER WHEN DRY MILLING OF ADDITIVE MANUFACTURED TI-6AL-4V TITANIUM ALLOY

**TOMAS TRCKA, ALES POLZER**

Brno University of Technology, Faculty of Mechanical Engineering, Institute of Manufacturing Technology, Brno, Czech Republic

**DOI: 10.17973/MMSJ.2021_6_2021006**

**e-mail: 153306@vutbr.cz**

Components with generally shaped surfaces requiring higher surface quality and dimensional accuracy are, in most cases, machined. Specifically, milling technology is involved very often, which can be supplemented by finishing operations. Besides standard ball-nose end mills, circle segment end mills are modern type of cutter that has begun to be used with the development of advanced computer aided machining software, that allows to work with these shaped tools. In this research, comparing the performance of these two modern shaped end mills was investigated. One tool was a commercially available coated solid carbide circle segment end mill. A second prototype end mill with the same profile but different geometry was made with a PCD insert, that additionally had a chipbreaker produced by laser technology. Machining was carried out on the workpiece material the Ti-6Al-4V that was manufactured by additive manufacturing (AM) technology – selective laser melting (SLM). The titanium complex parts are generally used in the transport industries and medicine. Milling tests were performed under dry cutting conditions. The evaluation was based on the force load, the roughness of the machined surface and tool wear. The higher total forces were measured by the tool with a PCD insert, because a different tool geometry was used, despite the use of integral chipbreaker, which allows a partial change of the cutting geometry of the insert. The geometry of end mills with brazed insert is limited by the production process.

**KEYWORDS**

circle segment end mill, laser technology, chipbreaker, Ti-6Al-4V, PCD, additive manufacturing.

## 1 INTRODUCTION

Machining of complex shaped surfaces is usually carried out by means of ball-nose or toroidal end mills with different corner radii.

The circle segment end mills constitute a new special type of milling cutter for 5-axis milling which enable reducing of machining times significantly and at the same time increasing the quality of the machined surface, thus minimizing the costs of possible polishing. Their primary use is mainly focused on pre-finishing and finishing operations of complex parts (turbine blades, mold-making etc.) [Emuge Corporation 2020 *II*] [Hoffmann Group].

The world-unique end mills were included in the FRANKEN production line and exhibited at the *International Engineering Fair (IMT)* in Brno in 2016, as the mentioned circle segment cutters. Company Garant (Hoffmann Group) calls the given machining strategy *PPC* (*Parabolic Performance Cutting*) [Hoffmann Group].

On mills is ground the large radius in the cutting area – a circle sector of effective radius size **R**, which can be seen on the left cutter in Fig. 1 [Bremstahler 2017] [Hoffmann Group]. The circle segment end mills by Emuge Corporation are in more detail divided according to the type and application options into shapes: lens-shape, barrel-shape, oval form and taper form [Bremstahler 2017] [Emuge Corporation 2020 *II*]. The above-mentioned manufacturer, together with WNT, states that circle segment cutters can simulate ball-nose end mills with a diameter of 12 to 3,000 mm or even more [Bremstahler 2017] [Emuge Corporation 2020 *II*] [WNT: Ceratizit Group 2017].

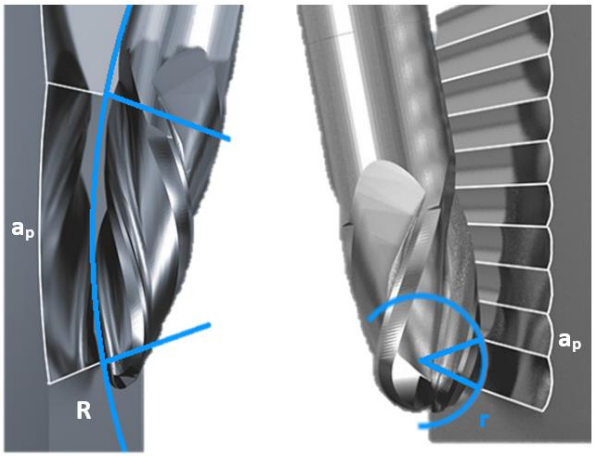


**Figure 1.** Different Value of $a_p$ For Circle Segment End Mill (left) and Ball-nose End Mill [Hoffmann Group].

Shorter machining times are achieved thanks to the larger stepover ($a_p$) - see Fig. 1. In the product video of the company Emuge is reported that 90 % of the total time is saved when finishing a conical pocket (36 seconds vs. 6 minutes and 15 seconds of a ball end mill) [Emuge Corp 2016] – in Fig. 2. The figure on the right represents the state of the entire pocket machined with the circle segment cutter, while the pocket on the left machined with the ball end mill represents the machining state at the same time.

**Figure 2.** Comparison of the Machined Surface with a Conventional Milling Cutter (left) and Oval-Form Circle Segment Cutter (right) [Emuge Corp 2016].

Conventional machining strategies are used for ball end mills, while new machining strategies and modern 5-axis milling machines must be used for the segment end mills. This is the disadvantage of the given tools, as the CAD/CAM software support is necessary and it has to support and compute the cutting curve (geometry) of the cutter or 3D model of workpiece, as in machining in Fig. 3. These include for example Mastercam or hyperMILL MAXX [Emuge Corp 2016], [Emuge Corporation 2020 *II*], [Hoffmann Group], [WNT: Ceratizit Group 2017].

The circle segment end mills generally represent a gap of knowledge, as they are still a recent revolutionary innovation that is not entirely industrialized and based on studies. With constantly developing machining technologies, more modern CNC machines, a growing percentage of all manufactured parts with complex shaped surfaces, it can be assumed that the end mills will be used more and more.

Diamond – the chemically metastable form of carbon at room temperature and standard atmospheric pressure – has become the standard material used for cutting tools..Nowadays, is a natural diamond successively replaced by an man-made - synthetic diamond, what also increases their availability. A synthetic polycrystalline diamond (PCD) produced by HPHT (high-pressure high-temperature) process is the most used diamond material for milling operations. The high fracture toughness of the tool is required for this type of machining technology [DAVIS 1995] [Tso 2002]. Another motivation of the work is also that diamond cutting material has not been applied to the given cutters so far, even though polycrystalline diamond has been preferred for machining of titanium alloys by many studies [Amin 2007], [Corduan 2003], [Li 2013], [Nabhani 2001], [Oosthuizen 2011], [Shokrani 2012], [Su 2012].

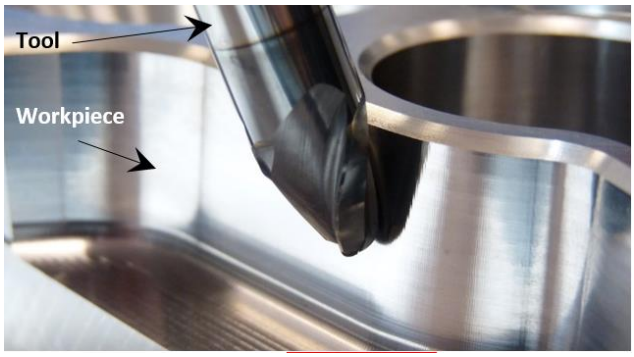


**Figure 3.** Machined Surface with a Taper Form of Circle Segment Cutter [Emuge Corp 2016].

However, the requirements for sharpening and machining increase due to PCD specific machinability, what is important fact for producers of cutting tools using diamond-based materials. In the past, the material was sharpened only by conventional grinding. In this technology, diamond grains bounded in the grinding wheel act on approximately equally hard PCD grains [DAVIS 1995]. Modern machining of these materials is based on unconventional machining methods. The diamond cutting insert is machined in a different way than by the cutting wedge. Standard PCD blank includes cemented tungsten carbide substrate, which provides cobalt as a binder during sintering process [Elementsix 2017] [Halpin 2015]. The presence of cobalt makes PCD electrically conductive, which allows sharpening by electrical technology. However, these technologies do not allow the optimal manufacturing of the integral chip breaker on the face of PCD insert, since the manufacturing is complicated compared to the production of the chip breaker in the insert of cemented tungsten carbide [Fraga da Silva 2017] [Soares 2017]. It is the application of laser technology in machining that enables more efficient chip breaker production [Hofmeister 2017] [Soares 2017]. Acting high-energy laser beam converts the solid state of PCD into gaseous, so-called cold ablation [Hofmeister 2017]. The high value of repetition rate corresponds to the large volume of material removed. A small value of pulse durations in picoseconds minimizes the heating/residual damage on the surrounding material [Zeman 2017]. The study of optimal sharpening technology and sharpening parameters of diamond-based cutting material (difficult-to-cut material) is still a topical science field as well as soldering conditions, tool geometry or specific conditions during machining, e.g. cryogenic cooling, dry machining etc. [Schoop 2017].

The present study is an application of circle segment cutters with a taper form, involving the comparison of two materially different cutters in the same application. The circle segment end mill with PCD inserts including integral chip breaker (labelled as *DP* tool) was designed, which was compared with a conventional coated cutter of the same cutting profile made of sintered carbides (labelled as *HC* tool). Problems with continuous chips do not occur during milling. However, in many cases it is advisable to reduce the cutting forces (the temperature in the cutting zone) due to the required quality of the machined surface, dimensional accuracy, etc. - for example in thin-walled parts [Hofmeister 2017]. Not only these parameters can be influenced by the chip breaker, hence this study is dedicated to this entity when milling [Zeman 2017]. The main response was the machining process itself with measurement of cutting forces (piezoelectric dynamometer Kistler 9257B) and analysis of the roughness of the machined surface of the part made by 3D printing.

## 2 MATERIALS, DESIGN AND EXPERIMENTAL SETUP

### *2.1 Workpiece*

The goal of the industry should be generally minimizing the acquisition costs of a given component, which are high for titanium components. The solution is to increase in efficiency of the cutting process, but also to reduce the *buy-to-fly* ratio, a term very often used in additive manufacturing technologies, which can in these technologies get this number into the order of units. The *buy-to-fly* ratio (the ratio of mass between the raw material used to produce a part and the mass of the final part) is given for titanium aircraft parts in the range of 12–25:1 for traditional manufacturing methods, while 3–12:1 for titanium parts produced by AM processes [Liu 2019]. The used method also has a considerable advantage in storage and the unused powder can be reused [Liu 2019]. On the other hand, the extraordinary huge price of fine powders for the 3D printing compared to other semi-finished products (sheet, bar, plate etc.) for the production of titanium components and input raw materials for the production of titanium ($TiO_2$ or $TiCl_4$) is a disadvantage [Yan 2015].

For an innovative reason, an AM technology, specifically SLM (Selective Laser Melting), was used to produce the input component as a workpiece for this experiment. The material was a Ti-6Al-4V. It is widely used in aerospace, marine and offshore, vehicle, gas turbine, engines and biomedical industries due to its specific functional properties [Amin 2007], [Babik 2017], [Balazic 2007], [Ezugwu 2003], [Krishnaraj 2014], [Li 2013], [Oosthuizen 2011], [Pittalà 2018], [Pramanik 2014], [Rao 2018], [Safari 2014]. The used machine was an SLM 280 HL with a YLR fibre laser [Yan 2015]. The construction of the component took place in a protective inert atmosphere $N_2$.

With the SLM method, the maximum temperature of about 2,710 K is produced when the metal powder Ti6Al4V melts [Liu

2019]. The subsequent rapid cooling rate $10^4$–$10^6$ K/s [Liu 2019], [Yan 2015] is a prerequisite for diffusionless transformation and formation of alpha prime (α') martensite phase after 3D printing [Ali 2018], [Kim 2018], [Liu 2019], [Yan 2015]. At such cooling rates, a diffusional process is not possible, i.e. α + β transformation. This has an effect on the resulting residual stress of the part after 3D printing, which is given for the SLM method [Liu 2019] in the range of 100-500 MPa. Part of this stress is released after the sample is cut from the substrate plate.

In addition to the huge temperature gradient, the related influence is also the build temperature, which for the SLM method is mostly only by natural heating [Liu 2019], [Yan 2015]. In the case of another 3D printing technology - EBM (Electron Beam Melting) - the residual stress is very low, as the building temperature is in the range of 600-750 °C [Liu 2019], 640–700 °C [Yan 2015]. This also has a significant effect on the microstructure, since the quasi-isothermal annealing stage is held at the build temperature, whereas the stage of decomposition of metastable **α'** (complete or incomplete decomposition) depends on the temperature [Liu 2019].

In the case of SLM, it is advisable to subsequently perform the stress-relieving heat treatment to reduce the residual stress, which will also improve the fatigue properties of the material [Syed 2019]. In the study [Syed 2019] using the SLM method and stress-relieving heat treatment at 680 °C for 3 hours, a partial decomposition of a very fine acicular martensite (**α'**) phase within the prior-**β** grains to more stabilized **α+β** at the boundaries was observed.

Due to the mentioned aspects of the SLM method, the part was post-processed after 3D printing – blasting and subsequent stress-relieving heat treatment to reduce residual stress at 640 °C (below the temperature of phase transformation) for  hours. Cooling took place in a furnace. Subsequently, the sample was cut by WEDM from the base plate.

The performed metallographic analysis of the sample after 3D printing in Fig. 4 with respect to the technology SLM confirmed the microstructure formed by fine acicular martensite, which resulted in a diffusionless martensitic transformation of the **β** phase into a metastable (a non-equilibrium) phase **α'**. The printing temperature was only a heating of the process itself. Therefore, the equilibrium conditions were not maintained during the 3D building process. On the stress-relieved microstructure (Fig. 5) the fine transformed phase **β** with larger **α**-lath was analysed [Liu 2019]. Other studies indicate incomplete decomposition of metastable α' to a mixture of **α** + **β/α '** [Liu 2019], [Syed 2019]. The measured hardness of both samples is shown in the respective figures and the final shape of workpiece in Fig. 10.

### 2.2 *Cutting Tools*

The designed *DP* right-hand and two-toothed tool had the same cutting profile (Fig. 6) as a standard coated solid carbide (*HC*) three-toothed tool by EMUGE-FRANKEN (type 3540L.12250A) with a tolerance of profile ± 0.01 mm and AlCr multi-layer PVD coating for heat and wear resistance [Emuge Corporation 2020 *I*]. This tolerance was fulfilled in both cases and was essentially the only basic common condition. The tool body material of *DP* tool was also sintered carbide, which is more rigid than steel. Both tools differed only in the number of teeth, cutting material and geometry - see Fig. 7. Tool geometry is a complex term, which is also affected by the integral chip breaker. The *DP* tool was made in a brazed design. The laser technology was used, both for machining of an integral chip breaker and sharpening of the cutting edge.

PCD blanks are mainly manufactured in the form of circular flat plates, which contains a flat layer of polished PCD sintered to the base of the sintered carbides. Therefore, the production of a cutting edge with constant tool cutting edge inclination ($\lambda_s$) is not possible from this blank. The rake angles are defined only by the position of the seat in the tool body, where the insert is brazed. The axial rake angle of the tool with the flat face surface of insert, which is defined as the angle between the plane of the rake face and the tool axis, had the value of 5°. This meant a gradual engagement of the cutter into the workpiece and more positive tool rake geometry further from the tool tip in the tool side geometry plane (radial plane). Due to the flat face this tool side rake ($\gamma_f$) is a variable. Its value is increasing with increasing distance from the tip. The tool cutting edge angle ($\kappa_r$) is 70° for

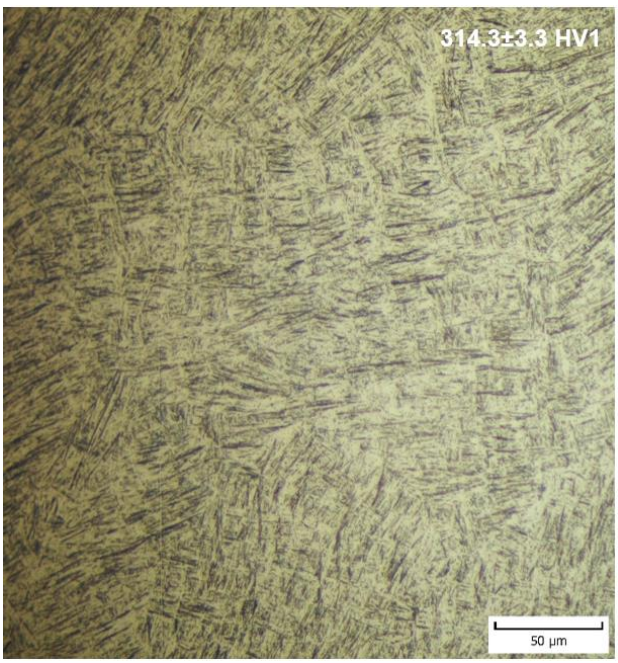


**Figure 4.** As-built Microstructure - Acicular **α'** Martensite Phase

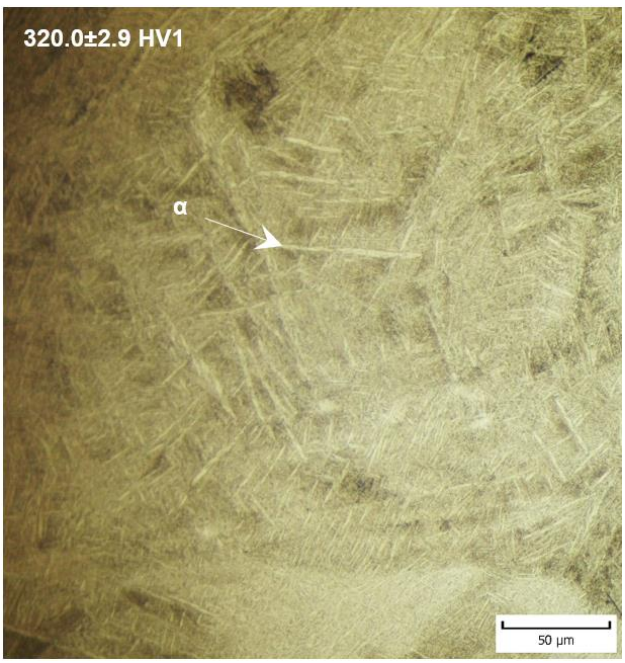


**Figure 5.** Microstructure After Stress-Relieving Heat Treatment - Phase **α** With Fine Phase **β**.

both end mills. Overall length of tools is 93 mm. Overhang of the tools from hydraulic tool holder is 45 mm.

Chip breaker has a groove shape that creates a more positive tool rake. The tool rake with respect to the insert has a constant value of 10° in the direction normal to the cutting edge. Together with tool body geometry (position of seat), the $\gamma_f$ is increased. The 3D chip breaker is designed with the 3D elements – drops, which are designed to reduce cutting forces – see Fig. 7. The aim is to create a space between the rake face and the leaving chip, thereby reducing the chip friction on the face of the insert and the related cutting force. Tool clearance angles (the first and second tool side clearance) have a variable value due to the complex cutting profile that passes through the tool axis.

The sort of PCD is CD-10M from company Ceratonia (Ceradite PCD), which is characterized by a diamond grain sizes of 10 µm. Overall thickness is 1 mm, because of strengthening of the body behind the insert in the area of the tool tip.

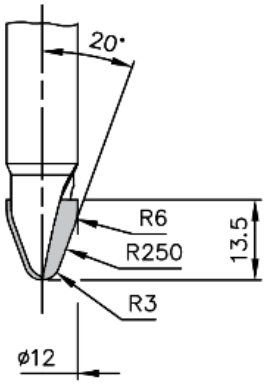


**Figure 6.** The Cutting Curve of the Taper Form of Circle Segment End Mills.

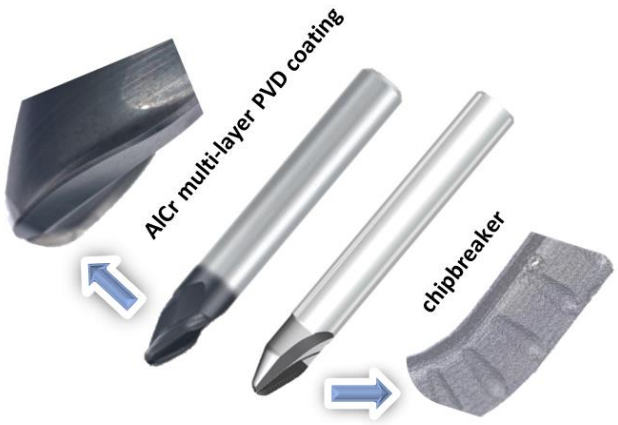


**Figure 7.** Solid *HC* End Mill (left) and 3D Model of Prototype *DP* Tool of The Same Cutting Profile with Polycrystalline Diamond (right).

The brazing process was carried out in a vacuum brazing furnace, which ensures a quality and strong joint through the controlled brazing process. Joint has to transfer the force load and heat between the insert and the tool body. Silver-based solder was used. Machine by company EWAG was used for sharpening as well as making the chip breaker. Sharpening was carried out on individual layers. Processing parameters for machining in the PCD layer were used for keeping high precision and minimization of damage on the surrounding material in the area of cutting edge, while parameters for higher productivity were used when machining the cemented tungsten carbide substrate (the second tool side clearance).

After production, the tools were inspected on the 3D optical system Alicona InfiniteFocus 5. The rounded cutting edge radius ($\mathbf{r_n}$) was comparable for both cutters - see Tab. 1. A lower value of $\mathbf{r_n}$ is more suitable for machining titanium alloys, since they are subject to a hardening of the surface layer. The **Ra** (the arithmetical mean deviation of the assessed surface roughness) value (according to ČSN EN ISO 4287) of a cutting edge (Fig. 8) was also lower for the *DP* tool as the laser beam passes through the grains of diamond. However, the roughness (**Sa**) of the chipbreaker of the PCD insert was higher than for the rake face of the *HC* tool as in the case of the flank faces. It is also caused by production technology - abrasive grinding (*HC*) and unconventional technology - laser (*DP*).

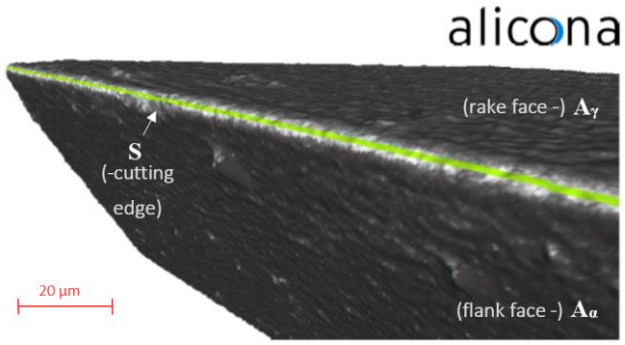


**Figure 8.** Cutting Edge of *HC* Tool with Marked Curve for Measuring **Ra** (green).

The size of the chipbreaker land width ($\mathbf{b_\gamma}$) on the rake face of the PCD insert, which had a model nominal value of 20 µm, was also analysed by measurement. However, for the manufactured *DP* tool, it differed greatly with the position of the insert. In some places it reached almost zero value, and on the contrary, in some places it exceeded the value of 40 µm - see Fig. 9.

| | Quantity | Unit | Value | |
|---|---|---|---|---|
| *Label* | | | *DP* | *HC* |
| **Rounded cutting edge radius** | $r_n$ | [µm] | 10.93±1.69 | 12.23±0.25 |
| **Arithmetical mean deviation of the roughness profile – measured on the cutting edge** | Ra | | 0.27 | 0.41 |
| **Arithmetical mean height of the scale limited surface - measured on the flank face** | Sa | | 0.26±0.30 | 0.19±0.23 |
| **Arithmetical mean height of the scale limited surface - measured in the chipbreaker** | Sa | | 0.46±0.63 | - |
| **Arithmetical mean height of the scale limited surface - measured on the rake face** | | | - | 0.38±0.47 |

**Table 1.** Measured Data of Both Tools Using the 3D Optical System Alicona InfiniteFocus 5.

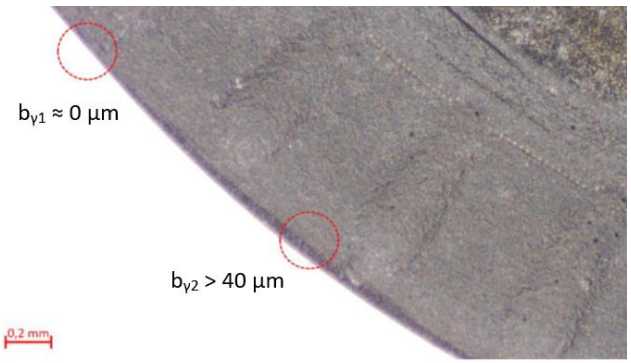


**Figure 9.** Different Land Width of The ChipBreaker of *DP* tool.

### 2.3 *Cutting Conditions*

A technology called *peel milling* is associated with the use of these types of end mills. It uses low radial depth of cut (5 to 10 % of the tool diameter) and on the contrary, a high value of axial depth of cut $\mathbf{a_p}$. The technology is suitable for machining difficult-to-cut materials, where a higher cutting temperature occurs in the cutting area and the generated heat is dissipated along the longer part of the cutting edge and is not concentrated in a small area of a tool. It is especially suitable for workpiece materials with low thermal conductivity, which also include titanium alloys [De Vos 2013], [Verellen 2007].

Emuge Franken recommend 0.05 to 0.2 mm as an allowance for finishing operations [Emuge Franken 2015]. The cutting conditions used for the experiment are shown in Tab. 2.

Generated heat during machining means difficulties in heat dissipation through the workpiece and chips of titanium alloys. The interface temperatures are extremely high and concentrated near the cutting edge [Ezugwu 2003]. Using the cutting fluids is one of the most common technique for improving machinability and decreasing tool wear, such as adhesion or diffusion [Shokrani 2012]. However, many emulsions have a major impact on the environment and the operator's health. Together with developing governmental regulations, it has resulted in increasing machining costs for different components [Ezugwu 2003] [Safari 2014] [Shokrani 2012]. Thermal damage of the cutting edge can occur when using a cutting fluid, such as thermal crack when milling [Kuljanic 1998].

Cryogenic cooling can be a solution to reducing the use of common cooling fluid [Ezugwu 2003] [Ezugwu 2005] [Pittalà 2018] [Shokrani 2012]. These gaseous coolants are relatively cleaner and more environmentally friendly than conventional cutting fluids.

In contrast, pre-heating (ion-beam, plasma heating and induction heating) of the workpiece can also significantly increase the tool life, as the workpiece becomes more machinable and reaches an optimal cutting temperature – this is another technique to eliminate the use of conventional cutting fluids [Shokrani 2012]. On the other hand, cutting tools can suffer from heat softening [Shokrani 2012].

In addition to the mentioned techniques, another technique to eliminate the use of conventional cutting fluids is dry machining, which is aimed at in this paper. To implement the dry machining, it is necessary to the choose the right cutting tool materials (progressive direction is using of new material [Ginta 2009]). PCD has four times higher thermal conductivity than tungsten carbide [Oosthuizen 2011] and higher hot hardness (the softening temperature) than other available cutting materials [Ezugwu 2003] [Oosthuizen 2011]. This helps to dissipate the generated heat while machining titanium alloys. In study [Nabhani 2001], PCD had the highest value of tool life and produced the best quality machined surface among CVD TiC/TiC-N/TiN triplecoated carbide and PCBN when dry milling of the Ti alloy.

The setup of the experiment, which was carried out on the CNC vertical milling machine FN 25 CNC with the HEIDENHAIN control unit together with a piezoelectric dynamometer Kistler 9257B, which was connected to a charge amplifier, is shown in Fig. 10.

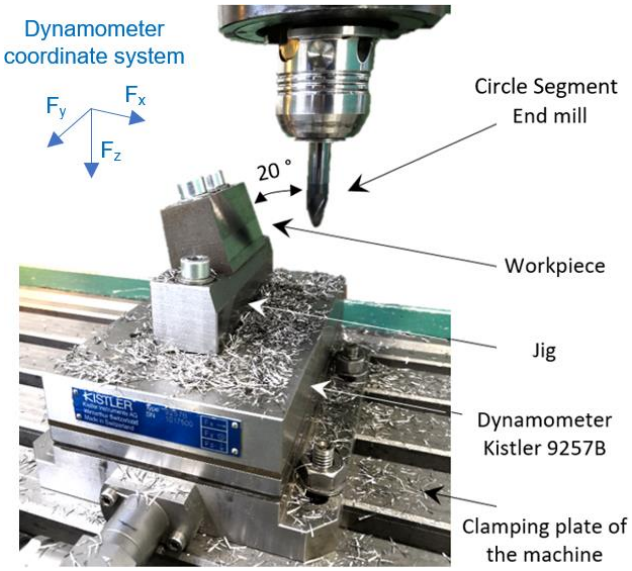


**Figure 10.** Workpiece and Dynamometer Setup.

| | Quantity | Unit | Value | | | |
|---|---|---|---|---|---|---|
| *Label* | | | *HC 65 m/min* | *HC 80 m/min* | *DP 120 m/min* | *DP 80 m/min* |
| **Number of teeth** | $n_t$ | [-] | 3 | | 2 | |
| **Cutting speed** | $v_c$ | [m·min$^{-1}$] | 65 | 80 | 120 | 80 |
| *Revolutions of the spindle* | *n* | *[min$^{-1}$]* | *1724* | *2122* | *3182.5* | *2122* |
| **Feed per tooth** | $f_z$ | [mm] | 0.04 | | | |
| *Feed rate* | $v_f$ | *[mm·min$^{-1}$]* | *207* | *254.6* | | *169.8* |
| **Axial depth of the cut** | $a_p$ | [mm] | ≈7 | | | |
| **Radial depth of the cut** | $a_e$ | [mm] | 0,2 | | | |
| **Down milling** | | | | | | |

**Table 2.** Cutting Conditions.

Filtering of raw data in standard *ASCII* exported from software DynoWare was evaluated using software Microsoft Excel. Each pass file included tens of thousands of lines, where each individual line contained the values of forces in individual axes at a given point in time. Before the measurement itself, it was necessary to set up some parameters of force recording. The sampling frequency was calculated with respect to the milling conditions and the required number of measurement points while the tool was in engagement. It was required that the dynamometer record 172 values per one revolution of the end mill. This is based on the requirement to record at least 5 values when end mill is in engagement under the cutting conditions used ($\mathbf{a_e}$, **D** and $\mathbf{f_z}$). Milling forces are not constant. Their values depend on passive deformation work in chip formation, thickness of chip etc. Therefore, subsequent filtration was obtained the mean value, from the maximum values during the cutter in engagement (from the machining time without the selected time at the beginning and end of the machined surface). The average length of the workpiece was 53 mm, which means that for each pass the average value for the statistics was calculated from almost 1000 values.

Optical microscope was used for identifying the wear mechanism(s) of the inserts. Surface roughness was analysed by the contact method on the Form Talysurf Intra 50 (manufactured by Taylor Hobson) with a radius of the scanning tip 2 µm.

## 3 RESULTS AND DISCUSSION

During and after dry machining, the following cutting-process issues were measured.

### 3.1 *Cutting Forces*

Depending on the given group of workpiece material and the stated value of the ultimate tensile strength (UTS) by the manufacturer of the *HC* tool, the recommended cutting speed can be assumed in the range of 60-80 m·min$^{-1}$ [Emuge Franken 2015]. For this reason, a pre-experiment was performed, which verified the reduction of force load for higher cutting speeds - see detailed Fig. 11 as well as passes 8 and 9 in Fig. 12. Thus, a cutting speed of 80 m·min$^{-1}$ for the *HC* tool was selected for the next measurements.

The total force exerted by a cutting part (**F**) is calculated from a relation (1). The passive force $\mathbf{F_p}$ acting in the z-axis direction of dynamometer is equal to measured force $\mathbf{F_z}$. Active force $\mathbf{(F_a)}$ is the force resultant in the radial plane *xy* of measured $\mathbf{F_x}$ and $\mathbf{F_y}$ forces and at the same time of cutting force $\mathbf{(F_c)}$ and normal cutting force $\mathbf{(F_{cN})}$.

$$F = \sqrt{F_x^2 + F_y^2 + F_z^2} = \sqrt{F_a^2 + F_p^2} = \sqrt{F_c^2 + F_{cN}^2 + F_p^2} \qquad (1)$$

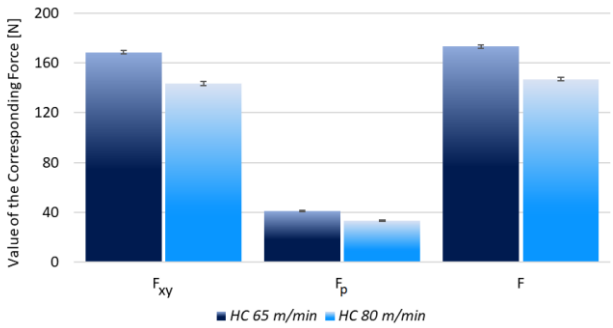


**Figure 11.** Forces During Machining with *HC* Tool with Different Cutting Speeds.

The curves of the dependence of the total force exerted by a cutting part on cutting time are shown in Fig. 12. The disadvantage of the tool with brazed inserts is that for small diameter cutters and inserts that passes through the tool axis it is not possible to design more than a two-tooth tool, while solid carbide cutters start with 3 teeth. To maintain the same machining productivity, a cutting speed of 120 m·min$^{-1}$ was used for the *DP* tool so that the feed rate was the same as the *HC* tool (see Tab. 2). This makes it possible to compare both tools for practice in a quality way.

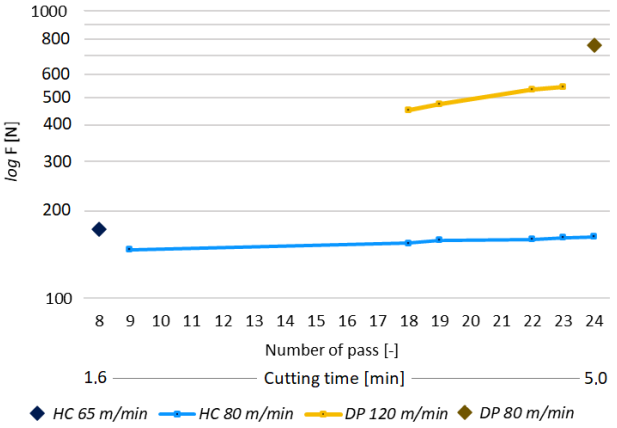


**Figure 12.** Dependence of Total Forces on the Number of Passes.

The curve for the *DP* tool starts at the 18$^{th}$ pass, because with the produced prototype tool there was repeated rubbing of the tool body against the workpiece (see Fig. 13 and 14). The tool was not manufactured according to a drawing and 3D model documentation. The cutting diameter was almost identical to the diameter of the tool body. The tool was corrected by the manufacturer twice by grinding off the body. This explains the complexity of producing a given type of cutter compared to the *solid* tool.


**Figure 13.** Grinded Off Part of Body (green) and Repeated Rubbing of *DP* Tool Body (red).

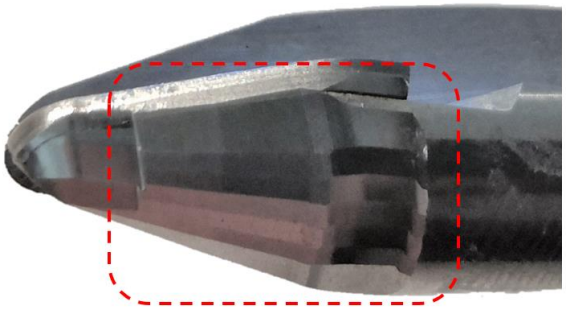

**Figure 14.** Another Grinded Off Part of Body.

The total forces **F** for the *DP* tool were several times higher than for the *HC* end mill. This was mainly due to the different tool geometry. At the beginning of the experiment, there was a huge adhesion of the workpiece material on the flank face, which appeared during the whole experiment - see chapter 3.3 and Fig. 16 to 20. This could also be caused by unsuitable sharpening and too low tool side clearances ($\alpha_{f1}$ and $\alpha_{f2}$). Another factor is undoubtedly the method of cooling, which was without cooling (dry machining). The changing size of the land width, which changed fundamentally within very small sections of the cutting edge (Fig. 9), has significant effect for cutting forces.

As stated above, with the brazed variant of the end mill (*DP* tool), it is not possible to make a variable tool cutting edge inclination ($\lambda_s$) and such a large positive $\lambda_s$ for a smooth and gradual engagement as for an *HC* tool. The only thing that can be structurally adjusted for such brazed milling cutters, where the cutting edge passes through the tool axis, is the axial rake angle (5°). Such tilting of the insert defines the rake angle in tool side geometry plane (radial plane) - the tool side rake ($\gamma_f$). It is zero at the tip of the tool as it passes through the axis and increases with increasing tool tip axial distance. The higher the axial angle, the greater the difference between the $\gamma_f$ at the tip (0°) and at the maximum diameter (12 mm). This geometry can be changed by modifying the rake face of the insert - a chipbreaker, which can make the given geometry more positive. However, the tool cutting edge inclination cannot be influenced by the chipbreaker in this case. In contrast, a conventional *HC* tool has a variable $\lambda_s$ in the range of 20-30° [Emuge Corporation 2020 *I*]. This significantly changes the chip formation conditions, as evidenced by the results. Grinding the profile into solid material has the advantage of being able to select suitable tool geometry – the case of the *HC* tool.

In terms of force load, the *DP* tool was used at 80 m·min$^{-1}$ (761.228 ± 2.181 N) at the end of the experiment to compare with the *HC* tool (146.964 ± 1.546 to 163.044 ± 1.800 N) under the same cutting conditions.

For both tools, a higher cutting speed $v_c$ means a reduction in the total force **F**.
. The *DP* tool had an increase of total force of 20 % in 6 passes, while *HC* tools had a percentage increase in load of only 11 % at 2.5 times higher cutting time. It is also supported by different cutting speeds. The experiment will be further developed.

### 3.2 Surface Roughness

Surface integrity is a key property in the functional performance of machined parts and assembled engineering components.

An increase in the cutting speed meant an increase in the **Ra** value in feed direction for both tools – see Fig. 15. One explanatory variant may be to increase the temperature in the cutting zone. This results in higher adhesive wear (adhesion of the workpiece material to the tool) and consequent deterioration of the machined surface, both in terms of dimensional accuracy and the adhering material in the form of deposits. Another explanation could be due to higher cutting force, that caused smoothing of the machined surface by formed chips during down milling. Higher cutting force meant lower **Ra** within the same tool. In the comparison of two types of tool, **Ra** could be affected by the tool wear. However, the wear of *HC* tool was very consistent throughout the experiment - see chapter 3.3. On the other hand, textured surfaces of implants integrate better with bone via osseointegration process compared to smooth surfaces [Babik 2017].

The growing trend is also in accord with the study [Amin 2007] Increasing speed meant an increase in average surface roughness Ra, which was still lower using PCD inserts compared to that using uncoated WC-Co. That was due to lower wear rate and smaller chatter in the case of PCD. On the contrary, research [Yang 2012] shows that the **Ra** value decreases with increasing cutting speed. Higher **Ra** values were achieved in the feed direction than in the axial depth of cut direction. In the same range of $v_c$ (up to 375 m·min$^{-1}$), the declining trend was the same in the research [Li 2013]. However, for higher cutting speeds, the Ra value increased again.

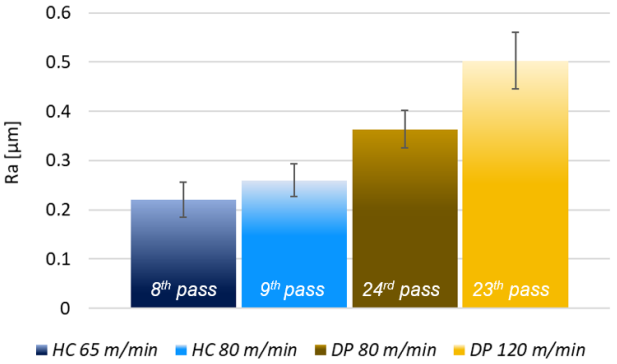


**Figure 15.** **Ra** Values of Machined Surface both tools and different cutting speeds.

### 3.3 Tool Wear

Measuring of cutting forces is one of the important experimental measurements in mechanical engineering. This measurement is an indirect measurement of the wear of the milling cutters. The state of wear of the cutting edge affects the size of the deformation work as well as friction work

Fig. 16 and 20 represent the wear of the *DP* tool, which was caused mainly by the adhesion mechanism. Adhered material was detected and was formed up to BUE. Oosthuizen [Oosthuizen 2011] confirmed that the BUE is the material of the workpiece. β phase with BCC lattice has strong tendency to adhere - [Kuljanic 1998]. Fig. 17 shows the adhered material on the flank face of *DP* tool. In the following measurement in Fig. 19, the adhered material was found in other positions. They were torn off after reaching a certain limit. As a result, this adhered layer in the form of a BUE was continuously forming and disappearing. This also generated more smeared material particles on the surfaces.

The wear of the *HC* tool at the end of the experiment can be seen in Fig. 21 and 22, where the cutting edge is mainly chipped.

## 4 CONCLUSION

The conclusion can be evaluated from two perspectives. The first is in terms of comparing *DP* and *HC* of the tool, where greater total forces were measured by the *DP* tool, because a different tool geometry was used and the results were also affected by the initial problems caused by the production of the tool. The geometry of end mills is very limited by the production technology together with the cutting profile. The design of chipbreakers, which allows the cutting geometry of the tool to be partially changed, was aimed at reducing the interface between the tool and the outgoing chip, achieving a more positive geometry while maintaining the rigidity of the tool. However, the production of a chipbreaker is also difficult, as shown by the changing size of the land width, which changed fundamentally within very small sections of the cutting edge (from almost 0 values to 40 µm). In some places, its large value even exceeded the value of the chip thickness, thus avoiding the effect of the chip breaker, as the chip did not even get into it.

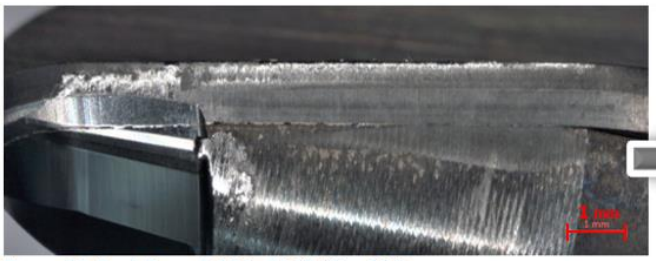


Figure 16. Flank Face of *DP* End Mill After 10 Passes.

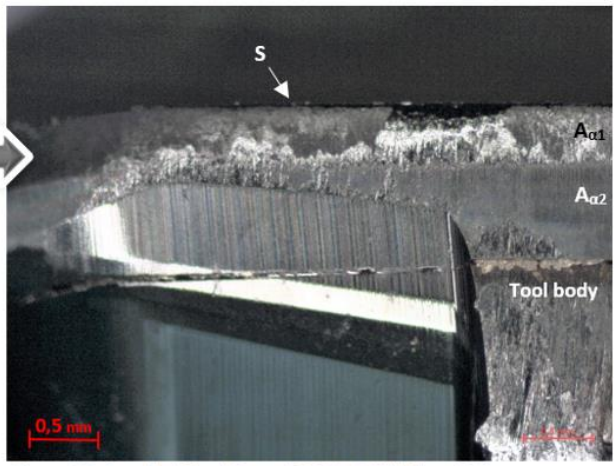


Figure 17. Detailed Flank Face of *DP* End Mill After 10 Passes.

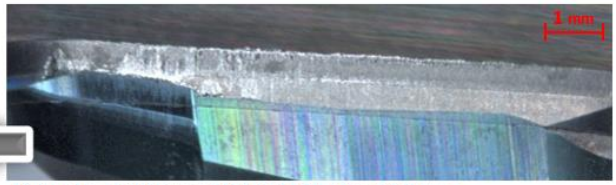


Figure 18. Flank Face of *DP* End Mill After 24 Passes.

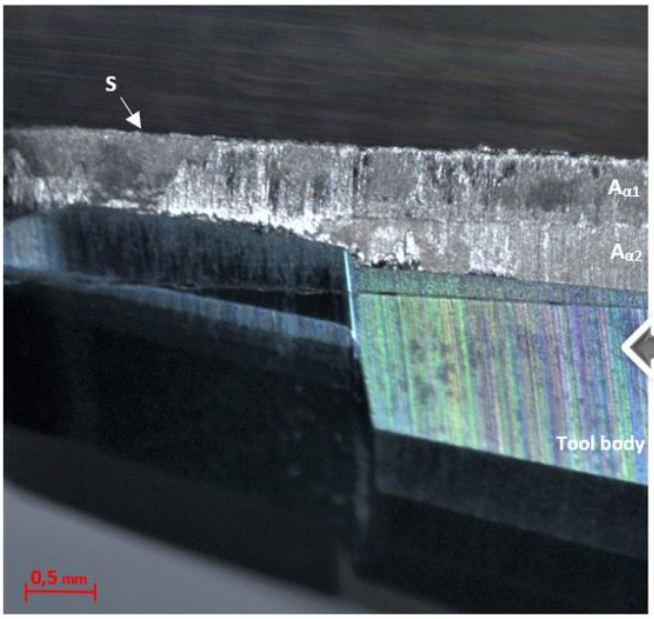


Figure 19. Detailed Flank Face of *DP* End Mill After 24 Passes.

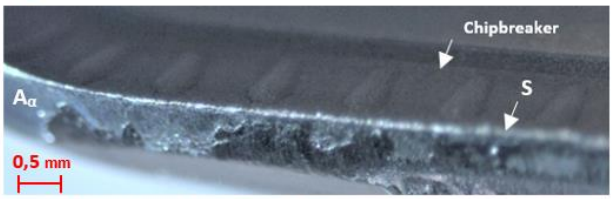


Figure 20. Cutting edge of *DP* End Mill After 24 Passes.

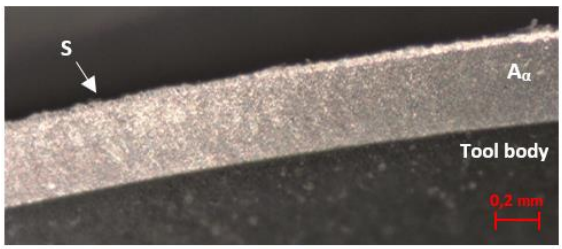


Figure 21. Flank Face of *HC* End Mill After 24 Passes.

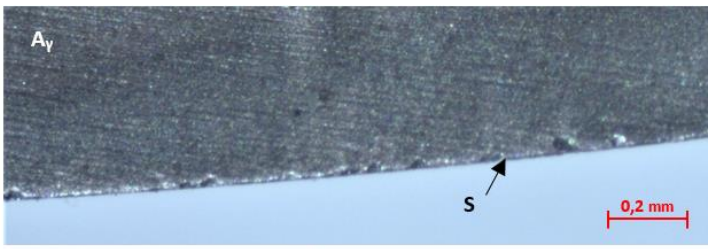


Figure 22. Rake Face of *HC* End Mill After 24 Passes.

The cutting force analysis determined that a higher cutting speed $\mathbf{v_c}$ meant a reduction in total force **F** and an increase in **Ra** (*DP* 0.364±0.038 µm → 0.503±0.057 µm and *HC* 0.221±0.035 µm → 0.260±0.034 µm) for both tools. The production of a tool with brazed insert is more complicated than a standard solid carbide tool.

The second conclusion of the study is the benefit of the given solid *HC* circle segment end mills, which can simulate ball-nose end mills even with a diameter of 3,000 mm or more. The general disadvantage of circle segment cutters with taper form is that the cutting speed varies within the cutting profile. However, the geometry of the tool can be selected with this factor in mind and adapted to the given location on the contour. The evidence is the variable tool cutting edge inclination ($\boldsymbol{\lambda_s}$) in the case of these cutters. Another disadvantage is more complex programming, but CAM machining strategies have been developed specifically for these tools by Open Mind [Bremstahler 2017], [WNT: Ceratizit Group 2017]. CNC machines must also handle higher loads than traditional ball end mills caused by higher stepover [Bremstahler 2017]. However, the machine tool manufacturer Hermle [Bremstahler 2017] also collaborated on the development of the tools, so the tools also have support in terms of machines. On the contrary, the advantages can be found in reducing machining times significantly and at the same time increasing the quality of the machined surface, thus minimizing the cost of any further finishing operations.

A possible effective application of the diamond cutting material in the case of modern circle segment cutters for machining of titanium alloys can be found in the CVD diamond coating allowing the use of optimal tool geometry, as in the case of solid carbide tools.

**ACKNOWLEDGMENTS**

This article was supported and co-financed from a specific research FV 19 – 09 called “Research in the field of milling of general shaped surfaces of material used in healthcare using CNC machines”.

**REFERENCES**


[Ali 2018] Ali, H., Ghadbeigi, H. and Mumtaz, K. Effect of scanning strategies on residual stress and mechanical properties of Selective Laser Melted Ti6Al4V. *Materials Science and Engineering: A* [online]. 2018, Vol. 712, pp 175-187 [cit. 2020-01-25]. DOI: 10.1016/j.msea.2017.11.103. ISSN 09215093.

[Amin 2007] Amin, A.K.M.N., Ismail, A.F. and Khairusshima, M.K.N. Effectiveness of uncoated WC–Co and PCD inserts in end milling of titanium alloy—Ti–6Al–4V. *Journal of Materials Processing Technology*, October 2007, Vol.192-193, pp 147-158. ISSN 0924-0136.

[Babik 2017] Babik, O., Czan, A., Holubjak, J., Kamenik, R. and Pilc, J. Identification of Surface Characteristics Created by Miniature Machining of Dental Implants Made of Titanium Based Materials. *Procedia Engineering*, 2017, Vol.192, pp 1016-1021. ISSN 1877-7058.

[Balazic 2007] Balazic, M. and Kopac, J. Improvements of medical implants based on modern materials and new technologies. *Journal of Achievements in Materials and Manufacturing Engineering*, December 2007, Vol.25, No.2., pp 31-34. ISSN 1734-8412.

[Bremstahler 2017] Bremstahler, A. More line spacing when finishing (in Czech). *MM Prumyslove spektrum,* 2017, Vol. 6, pp 74. ISSN 1212-2572.

[Corduan 2003] Corduan, N., Himbart, T., Poulachon, G., Dessoly, M., Lambertin, M., Vigneau, J. and Payoux, B. Wear Mechanisms of New Tool Materials for Ti-6AI-4V High Performance Machining. *CIRP Annals*, 2003, Vol.52, No.1., pp 73-76. ISSN 0007-8506.

[DAVIS 1995] DAVIS, J.R. Tool Materials. ASM Specialty Handbook. Ohio: ASM International, 1995. ISBN 0-87170-545-1

[De Vos 2013] De Vos, P. Technology Handbook: Dynamic Milling - Using the Compensation Approach (in Czech). *MM Prumyslove spektrum,* 2013, Vol. 7, pp 82. ISSN 1212-2572.

[Elementsix 2017] *Elementsix*. Synthetic Polycrystalline Diamond (PCD). Elementsix [online]. c2017 [20. 5. 2019]. Available from https://www.e6.com/en/Home/Materials+and+products/Synthetic+Polycrystalline+Diamond+%28PCD%29/.

[Emuge Corp 2016] EMUGE Circle Segment & Trochoidal Milling Strategies. In: *Youtube* [online]. EMUGE Corp, 2016 [cit. 2020-05-02]. Available from: https://www.youtube.com/watch?v=OvAAu31RC0I

[Emuge Corporation 2020 *I*] Circle segment cutters: Taper Form <45°: 3540L.12250A. *EMUGE* [online]. West Boylston: Emuge Corporation, 2020 [cit. 2020-12-23]. Available from: https://www.emuge.com/products/end-mills/circle-segment-cutters/taper-form-cutter/3540l12250a

[Emuge Corporation 2020 *II*] Circle segment cutters: 5-Axis Milling Tooling. *EMUGE* [online]. West Boylston: Emuge Corporation, 2020 [cit. 2020-05-02]. Available from: https://www.emuge.com/products/end-mills/circle-segment-cutters

[Emuge Franken 2015] Franken: Milling technology - Catalogue 250. *Emuge Franken* [online]. 2015 [cit. 2020-12-23]. Available from: http://250.ef-catalogues.com/index.html

[Ezugwu 2003] Ezugwu, E.O., Bonney, J. and Yamane, Y. An overview of the machinability of aeroengine alloys. *Journal of Materials Processing Technology,* March 2003, Vol.134, No.2., pp 233-253. ISSN 0924-0136.

[Ezugwu 2005] Ezugwu, E. O. Key improvements in the machining of difficult-to-cut aerospace superalloys. *International Journal of Machine Tools and Manufacture*, October 2005, Vol.45, No.12-17., pp 1353-1367. ISSN 0890-6955.

[Fraga da Silva 2017] Fraga da Silva, T., Soares, R. B., Jesus, A. M. P., Rosa, P. A. R. and Reis, A. Simulation Studies of Turning of Aluminium Cast Alloy Using PCD Tools. Procedia CIRP, 2017, Vol.58, pp 555-560. ISSN 2212-8271.

[Ginta 2009] Ginta, L.T., Lajis, M.A. and Amin, A.K.M.N. The Performance of Uncoated Tungsten Carbide Insert in End Milling Titanium Alloy Ti-6Al 4V through Work Piece Preheating. *American Journal of Engineering and Applied Sciences*, 2009, Vol.2, pp 147-153. ISSN 1941-7020.

[Halpin 2015] Halpin, T. and Haas-Wittmüss, J. Special synthetic diamond for machining (in Czech). MM Prumyslove spektrum [online]. 2015, 1 [20. 10. 2019]. Available from https://www.mmspektrum.com/clanek/specialni-syntetickydiamant-urceny-pro-obrabeni.html.

[Hoffmann Group] Dynamic 5-axis milling with PPC Garant mills and PPC cutting inserts: For shorter process times and the highest surface quality during milling (in Czech). *Hoffmann Group* [online]. [cit. 2020-03-23]. Available from: https://www.hoffmann-group.com/CZ/cs/hot/company/garant/garant-innovationen/tonnenfraeser-ppc

[Hofmeister 2017] *Hofmeister*. Adapting of chip breaker on the cutting tool for specific machining conditions. MM Prumyslove spektrum [online]. 2017, 5 [24. 10. 2019]. Available from https://www.mmspektrum.com/clanek/adaptace-utvarece-na-reznem-nastroji-pro-konkretni-podminky-obrabeni.html.

[Kim 2018] Kim, Y.-K., Park, S.-H., Kim, Y.-J., Almangour, B. and Lee, K.-A. Effect of Stress Relieving Heat Treatment on the Microstructure and High-Temperature Compressive Deformation Behavior of Ti-6Al-4V Alloy Manufactured by Selective Laser Melting. *Metallurgical and Materials Transactions A* [online]. 2018, Vol. 49, No. 11, pp 5763-5774 [cit. 2020-01-25]. DOI: 10.1007/s11661-018-4864-0. ISSN 1073-5623.

[Krishnaraj 2014] Krishnaraj, V., Samsudeensadham, S., Sindhumathi, R. and Kuppan, P. A study on High Speed End Milling of Titanium Alloy. *Procedia Engineering*, 2014, Vol.97, pp 251-257. ISSN 1877-7058.

[Kuljanic 1998] Kuljanic, E., Fioretti, M., Beltrame, L. and Miani, F. Milling Titanium Compressor Blades with PCD Cutter. *CIRP Annals*, 1998, Vol.47, No.1., pp 61-64. ISSN 0007-8506.

[Li 2013] Li, A., Zhao, J., Dong, Y., Wang, D. and Chen, X. Surface Integrity of High-speed Face Milled Ti-6Al-4V Alloy with PCD Tools. *Machining Science and Technology*, 2013, Vol.17, pp 464-482. ISSN 1532-2483.

[Liu 2019] Liu, S. and Shin, Y. Additive manufacturing of Ti6Al4V alloy: A review. *Materials & Design* [online]. 2019, Vol. 164 [cit. 2020-01-25]. DOI: 10.1016/j.matdes.2018.107552. ISSN 02641275.

[Nabhani 2001] Nabhani, F. Machining of aerospace titanium alloys. *Robotics and Computer-Integrated Manufacturing*, February 2001, Vol.17, No.1-2., pp 99-106. ISSN 0736-5845.

**[Oosthuizen 2011]** Oosthuizen, G.A., Akdogan, G. and Treurnicht, N. The performance of PCD tools in high-speed milling of Ti6Al4V. *The International Journal of Advanced Manufacturing Technology*, February 2011, Vol.52, No.9-12., pp 929-935. ISSN 0268-3768.

**[Pittalà 2018]** Pittalà, G.M. A study of the effect of $CO_2$ cryogenic coolant in end milling of Ti-6Al-4V. *Procedia CIRP*, 2018, Vol.77, pp 445-448. ISSN 2212-8271.

**[Pramanik 2014]** Pramanik, A. Problems and solutions in machining of titanium alloys. *International Journal of Advanced Manufacturing Technology*, February 2014, Vol.70, No.5-8., pp 919-928. ISSN 0268-3768.

**[Rao 2018]** Rao, Ch.M., Rao, S.S. and Herbert, M.A. Influence of Modified Cutting Inserts in Machining of Ti-6Al-4V Alloy Using PCD Insert. *Materials Today: Proceedings*, 2018, Vol.5, No.9., pp 18426-18432. ISSN 2214-7853

**[Safari 2014]** Safari, H., Sharif. S. and Izman S. Influence of Cutting Conditions on Surface and Sub-Surface Quality of High Speed Dry End Milling Ti-6Al-4V. *Jurnal Teknologi*, 2014, Vol.67, pp 131-135. ISSN 2180–3722.

**[Schoop 2017]** Schoop, J., Sales, W.F. and Jawahir, I.S. High speed cryogenic finish machining of Ti-6Al4V with polycrystalline diamond tools. Journal of Materials Processing Technology, December 2017, Vol. 250, pp 1-8. ISSN 0924-0136

**[Shokrani 2012]** Shokrani, A., Dhokia, V. and Newman, S.T. Environmentally conscious machining of difficult-to-machine materials with regard to cutting fluids. *International Journal of Machine Tools and Manufacture*, June 2012, Vol.57, pp 83-101. ISSN 0890-6955.

**[Soares 2017]** Soares, R. B., P. de Jesus, A. M, Neto, R. J. L., Rosa, P. A. R., Machado, M. and Reis, A. Machinability of an Aluminium Cast Alloy Using PCD Tools for Turning. In: Materials Design and Applications, Springer, Cham, March 2017, pp 329-346. ISBN 978-3-319-50784-2.

**[Su 2012]** Su, H., Liu, P., Fu, Y. and Xu, J. Tool Life and Surface Integrity in High-speed Milling of Titanium Alloy TA15 with PCD/PCBN Tools. *Chinese Journal of Aeronautics*, October 2012, Vol. 25, No. 5, pp 784-790. ISSN 1000-9361.

**[Syed 2019]** Syed, A. K., Ahmad, B., Guo, H., Machry, T., Eatock, D., Meyer, J., Fitzpatrick, M. E. and Zhang, X. An experimental study of residual stress and direction-dependence of fatigue crack growth behaviour in as-built and stress-relieved selective-laser-melted Ti6Al4V. *Materials Science and Engineering: A* [online]. 2019, Vol. 755, pp 246-257 [cit. 2020-01-25]. DOI: 10.1016/j.msea.2019.04.023. ISSN 09215093.

**[Tso 2002]** Tso, P.-L. and Liu, Y.-G. Study on PCD machining. International Journal of Machine Tools & Manufacture, February 2002, Vol.42, No.3, pp 331-334. ISSN 0890-6955

**[Verellen 2007]** Verellen, J. The Appeal Of Peel Milling. *Modern Machine Shop* [online]. Seco. Cincinnati: Gardner Business Media, 2007 [cit. 2019-05-24]. Available from: https://www.mmsonline.com/articles/the-appeal-of-peel-milling

**[WNT: Ceratizit Group 2017]** Circular segment cutters have productivity over a barrel. *WNT: CERATIZIT GROUP* [online]. Ceratizit UK & Ireland Ltd., 2017 [cit. 2020-04-28]. Available from: https://www.wnt.com/ie/news-detail/circular-segment-cutters-have-productivity-over-a-barrel-1659.html

**[Yan 2015]** Yan, M. and Yu, P. An Overview of Densification, Microstructure and Mechanical Property of Additively Manufactured Ti-6Al-4V — Comparison among Selective Laser Melting, Electron Beam Melting, Laser Metal Deposition and Selective Laser Sintering, and with Conventional Powder Metallurgy. *Sintering Techniques of Materials - InTech* [online]. 2015, pp 77-106 [cit. 2020-01-25]. DOI: 10.5772/59275. ISBN 978-953-51-2033-9. Available from: https://www.intechopen.com/books/sintering-techniques-of-materials/an-overview-of-densification-microstructure-and-mechanical-property-of-additively-manufactured-ti-6a

**[Yang 2012]** Yang, X., Ren, Ch., Wang, Y., and Chen, G. Experimental study on surface integrity of Ti-6Al-4V in high speed side milling. *Transactions of Tianjin University* [online]. 2012, Vol. 18, No. 3, pp 206-212 [cit. 2018-05-27]. DOI: 10.1007/s12209-012-1784-8. ISSN 1006-4982.

**[Zeman 2017]** Zeman, P. Research of progressive laser technologies (in Czech). MM Prumyslove spektrum [online]. 2017, 9 [25. 12. 2019]. Available from https://www.mmspektrum.com/clanek/vyzkum-progresivnich-laserovych-technologii.html.

**CONTACT:**

Ing. Tomas Trcka
Brno University of Technology,
Faculty of Mechanical Engineering,
Institute of Manufacturing Technology,
Technicka 2896/2, 616 69 Brno, Czech Republic
e-mail: 153306@vutbr.cz